Journal of Experimental and Theoretical Physics, Vol. 99, No. 4, 2004, pp. 766–775.
Translated from Zhurnal Éksperimental'noĭ i Teoreticheskoĭ Fiziki, Vol. 126, No. 4, 2004, pp. 887–897.

SOLIDS
Structure

Antiferromagnetic Resonance and Phase Diagrams of Gadolinium Ferroborate $GdFe_3(BO_3)_4$

A. I. Pankrats, G. A. Petrakovskiĭ, L. N. Bezmaternykh, and O. A. Bayukov

Kirenskiĭ Institute of Physics, Siberian Division, Russian Academy of Sciences, Akademgorodok, Krasnoyarsk, 660036 Russia

e-mail: pank@iph.krasn.ru

Received March 29, 2004

Abstract—Antiferromagnetic resonance in single crystals of rhombohedral gadolinium ferroborate $GdFe_3(BO_3)_4$ was studied. The frequency–field dependences of antiferromagnetic resonance over the frequency range 26–70 GHz and the temperature dependences of resonance parameters for magnetic fields oriented along the crystal axis and in the basal plane were determined. It was found that the iron subsystem, which can be treated as a two-sublattice antiferromagnet with anisotropy of the easy-plane type, experienced ordering at T = 38 K. At temperatures below 20 K, the gadolinium subsystem with the opposite anisotropy sign strongly influenced the anisotropic properties of the crystal. This resulted in a spontaneous spin-reorientation transition from the easy-plane to the easy-axis state at 10 K. Below 10 K, magnetic field-induced transitions between the states were observed. Experimental phase diagrams on the temperature–magnetic field plane were constructed for fields oriented along the crystal axis and in the basal plane. A simple model was used to calculate the critical transition fields. The results were in close agreement with the experimental values measured at T = 4.2 K for both field orientations. © *2004 MAIK "Nauka/Interperiodica".*

1. INTRODUCTION

Crystals whose magnetic subsystems are formed by ions of different kinds have interesting magnetic properties. These properties are especially pronounced in rare-earth magnets in which rare-earth ions interact with 3*d* iron family ions. Most rare-earth metal ions are strongly anisotropic, and the magnetic anisotropy of such crystals is as a rule determined by the competition of the anisotropic interactions of these groups of ions. This results in the appearance of spin-reorientation transitions, both spontaneous that occur when temperature changes and field-induced. Transitions of this type and magnetic phase diagrams have been thoroughly studied for rare-earth metal ferrite–garnets and orthoferrites [1].

Another class of crystals of rare-earth metal compounds of the general formula $RM_3(BO_3)_4$, where R is a rare-earth metal and M = Fe, Cr, Al, Ga, and Sc [2–5], has received much less attention. These compounds are of interest not only from the point of view of their magnetic properties: they offer promise as materials for laser techniques and second optical harmonic generation. The crystals have hantite rhombohedral structures, space group *R*32 [6]. The magnetic properties of rare-earth crystals of this class remain virtually unstudied. The temperature dependences of magnetization measured for polycrystalline $RFe_3(BO_3)_4$ samples, where R = Y, La, Nd, Eu, and Ho [6, 7], made it possible to suggest antiferromagnetic ordering in these compounds.

More detailed and informative studies have recently been performed for $GdFe_3(BO_3)_4$ single crystals [8]. Temperature dependence anomalies were observed for magnetization at about 10 and 40 K. In addition, the field dependences of magnetization contained jumps below 10 K when the field was directed along the crystal axis. These jumps were interpreted as spin flop transitions. On the basis of these data, a model of the magnetic structure of $GdFe_3(BO_3)_4$ was suggested in [8]; its reliability, however, is questionable. It is very difficult to unambiguously determine the magnetic structure of a crystal solely on the basis of magnetic measurements. The purpose of this work was to study the magnetic structure and phase transitions of gadolinium ferroborate $GdFe_3(BO_3)_4$ by the antiferromagnetic resonance method, which is very sensitive to the magnetic structure of crystals.

We stress that the $GdFe_3(BO_3)_4$ crystal is the first representative of the family of crystals with the hantite structure for which the magnetic structure and magnetic phase diagram were studied in detail. This crystal offers much promise for studies of this kind, because both magnetically active ions, Fe^{3+} and Gd^{3+}, are *S* ions. This circumstance is of special importance for resonance studies, because the corresponding resonance absorption should be fairly narrow.

2. EXPERIMENTAL DATA

We used $GdFe_3(BO_3)_4$ single crystals; the procedure for preparing them was described in [8]. Measurements

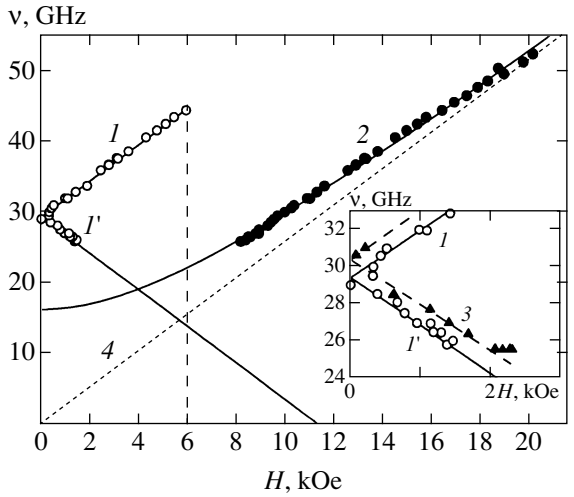

Fig. 1. Frequency–field dependence of antiferromagnetic resonance in $GdFe_3(BO_3)_4$ at $T = 4.2$ K and $\mathbf{H} \parallel c$. Line *4* corresponds to the paramagnetic dependence $\nu = \gamma H$. The initial portions of the dependences for (*1*, *1'*) $GdFe_3(BO_3)_4$ and (*3*) $GdFe_{3-x}Ga_x(BO_3)_4$ are shown in the inset.

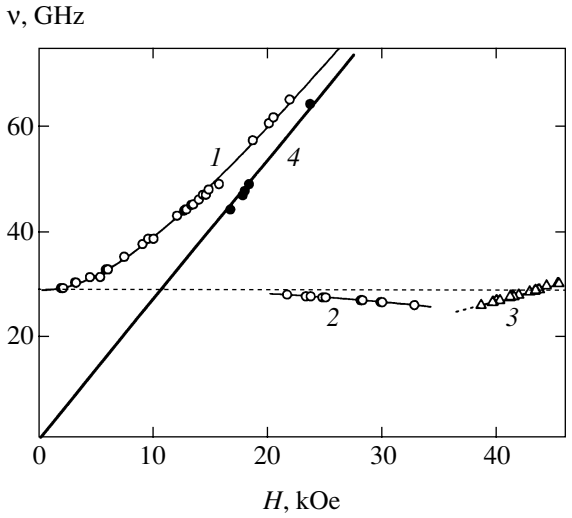

Fig. 2. Frequency–field dependences of antiferromagnetic resonance at $T = 4.2$ K, magnetic field is perpendicular to the crystal axis.

were performed for bulk single crystals with well-defined faceting of size up to 2 mm.

Magnetic resonance was studied over the frequency and temperature ranges 25–70 GHz and 4.2–60 K, respectively, using an automated magnetic resonance spectrometer with a pulsed magnetic field [9].

The frequency–field dependence of antiferromagnetic resonance measured at $T = 4.2$ K in a magnetic field directed along the principal crystal axis c is shown in Fig. 1. Two dependence regions can easily be distinguished. At low magnetic fields, we observe two oscillation branches (*1* and *1'*) whose frequencies linearly depend on the field and the line width does not exceed 110 Oe at 37 GHz for the best samples. Both branches have equal initial splittings of about 29 GHz; the frequency of one of them linearly increases as the field grows, and that of the other decreases. In fields higher than $H_c \approx 6.0$ kOe, both magnetic resonance branches disappear (the highest resonance frequency of the upper branch is about 44.4 GHz). In their place, one oscillation branch (*2*) appears; its frequency increases as the field rises, and its splitting is smaller than that of the first two oscillation branches.

The frequency–field dependences of antiferromagnetic resonance measured at 4.2 K for the magnetic field orientation in the basal plane are shown in Fig. 2. We observe two oscillation branches with the same initial splitting as for $H \parallel c$ (Fig. 1). The frequency of one of them (*1*) nonlinearly increases as the field grows stronger. The other branch (*2*) is a decreasing function. Its linewidth measured in a magnetic-field sweep is 6–8 times larger than that for the first branch, and its frequency slowly decreases as the field increases. In strong fields, an additional line is observed, due to a narrow resonance. The corresponding frequency is a slowly increasing function of magnetic field intensity (see curve *3* and triangles in Fig. 2).

The temperature dependences of resonance fields for the magnetic field oriented along the crystal axis were measured at frequencies of 26.11 and 44.48 GHz (Fig. 3). At the lower frequency, we observed resonance absorption corresponding to both the low- (line *1*) and high-field (line *2*) regions. In the low-field region, the resonance field first decreased to zero and then increased as the temperature grew. This resonance disappeared above approximately 8.5 K. The resonance

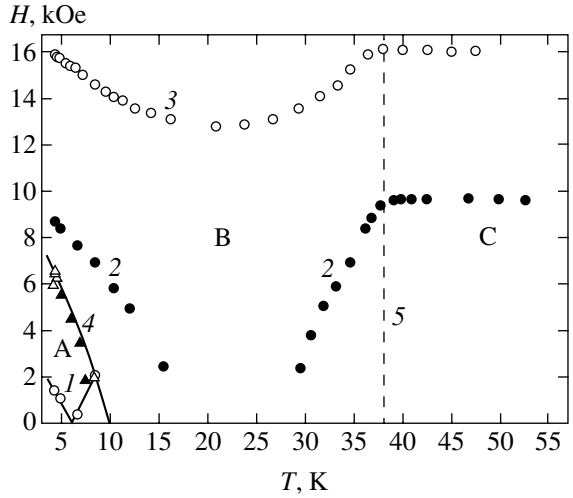

Fig. 3. Temperature dependences of resonance and critical fields at $\mathbf{H} \parallel c$ and frequencies of (*1*, *2*) 26.11 and (*3*) 44.48 GHz. State regions: A, easy-axis; B, easy-plane; and C, paramagnetic. Open and solid triangles are the antiferromagnetic resonance and magnetic measurement [8] data, respectively.

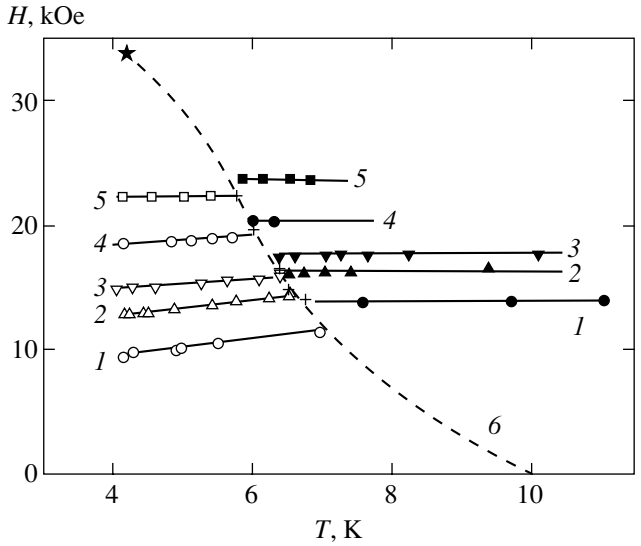

Fig. 4. Temperature dependences of resonance and critical fields at $\mathbf{H} \perp c$ and frequencies of (*1*) 38.63, (*2*) 44.32, (*3*) 47.04, (*4*) 57.55, and (*5*) 64.45 GHz. The dashed line *6* was drawn "by eye."

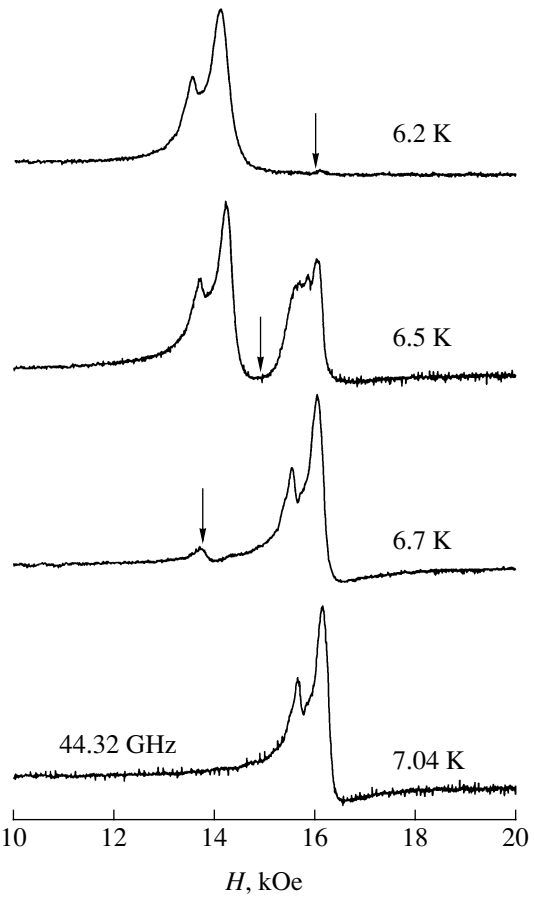

Fig. 5. Temperature-induced transformation of the resonance absorption spectrum at a 44.32 GHz frequency in the magnetic field perpendicular to the crystal axis.

field for the high-field resonance branch also sharply decreased to zero as the temperature increased to approximately 18 K. Over the temperature range 18–28 K, no resonance absorption was observed at this frequency. Starting with $T \approx 28$ K, resonance absorption reappeared, and the resonance field increased as the temperature grew and reached a plateau at $T \approx 38$ K. As the 44.48 GHz frequency was slightly higher than the highest frequency of the upper oscillation branch in the low-field resonance region, we only observed resonance absorption corresponding to the high-field branch over the whole temperature range. The temperature dependence of the resonance field was qualitatively similar to that characteristic of the lower frequency, namely, the resonance field first decreased and passed a minimum at about 20 K and then increased and reached a plateau close to 38 K.

The temperature dependence of the resonance parameters was different when the field was oriented in the basal plane of the crystal. The temperature dependences of the resonance fields measured at various frequencies are shown in Fig. 4. The fields first monotonically increase as the temperature of the crystal grows. Next, at a certain temperature, the resonance spectrum sharply changes, the temperature interval of these changes being less than 1 K. The transformation of the resonance spectrum measured at 44.32 GHz is shown in Fig. 5. The spectrum contains one inhomogeneously broadened line corresponding to branch *1* in Fig. 2 at temperatures up to about 6 K (the weak peak on the left wing of the resonance line is in our view an inhomogeneous peak). Additional resonance absorption appears at $T = 6.2$ K in higher magnetic fields above some critical value marked by an arrow in the figure. The critical field decreases as the temperature grows, and, at $T = 6.5$ K, the absorption spectrum contains two absorption lines. The low-field absorption line disappears as the temperature increases further, and only the high-field line remains.

The region of resonance spectrum transformation shifts to lower temperatures as the resonance frequency increases. The temperature dependence of the critical field is shown in Fig. 4 by crosses (line *6*). We also see that the resonance field of the high-field peak is independent of temperature to the right of line *6*. The frequency–field dependence for this crystal state is shown in Fig. 2 (line *4*); it can be approximated by a linear dependence starting at the origin.

3. RESULTS AND DISCUSSION

It is reasonable to assume that the magnetic properties of $GdFe_3(BO_3)_4$ are determined by the coexistence of two magnetic subsystems of iron and rare-earth metal ions interrelated by exchange interaction. An analysis of the resonance data obtained at $T = 4.2$ K leads us to conclude that the crystal at low temperatures in the ground state is an antiferromagnet with an easy anisotropy axis parallel to the principal crystal axis.

Indeed, if magnetic field H_0 is applied along the crystal axis and is lower than the critical spin flop transition field H_{sf}, the field dependences of the resonance frequencies have the form [10, 11]

$$\frac{\nu_{1,2}}{\gamma_\parallel} = \sqrt{(2H_E + H_A)H_A} \pm H_0\left(1 - \frac{\chi_\parallel}{2\chi_\perp}\right), \quad H < H_{sf} = \sqrt{(2H_E - H_A)H_A}. \tag{1}$$

For the spin flop phase, we have

$$\left(\frac{\nu_1}{\gamma_\parallel}\right)^2 = H_0^2\frac{2H_E(2H_E + H_A)}{(2H_E - H_A)^2} - 2H_E H_A, \quad \nu_2 = 0, \quad H > H_{sf}. \tag{2}$$

Here, H_E and H_A are the effective exchange and anisotropy fields, respectively, with respect to the crystal axis c ($H_A > 0$); $\chi_\parallel$ and $\chi_\perp$ are the antiferromagnetic susceptibilities along the principal axis and in the basal plane, respectively; and $\gamma_\parallel$ is the gyromagnetic ratio for the axial magnetic field direction. The solid lines in Fig. 1 are the theoretical dependences constructed according to (1) for oscillation branches *1* and *1'*. The dependence parameters are as follows: $\nu_{\parallel c} = \gamma_\parallel\sqrt{(2H_E - H_A)H_A} = 29.4 \pm 0.2$ GHz and $\gamma_\parallel(1 - \chi_\parallel/2\chi_\perp) = 2.55 \pm 0.05$ MHz/Oe. Using the $\gamma_\parallel = 2.808$ MHz/Oe value obtained from EPR measurements at room temperature, we obtain the susceptibility ratio $\chi_\parallel/2\chi_\perp = 0.081$, which is close to the experimental value 0.083 measured at $T = 4.2$ K [8].

The magnetic field value $H_c = 6.0$ kOe at which the oscillation branches described by (1) for $H < H_{sf}$ disappear at $T = 4.2$ K is close to the characteristic field $H_c = 6.15$ kOe corresponding to the magnetization jump observed in [8] and interpreted as a spin flop transition. However, oscillation branch *2* observed at this magnetic field orientation in fields higher than 6.0 kOe cannot be assigned to a resonance in the spin flop phase of an easy-axis antiferromagnet, primarily because the critical field H_c of the disappearance of the resonance of the easy-axis phase is much lower than the spin flop transition field $H_{sf} = 11.3$ kOe calculated by (1). In addition, the experimental frequency–field dependence in fields higher than 6.0 kOe cannot be approximated by Eq. (2) for the spin flop phase with any reasonable parameter values. At the same time, these data are well described by the dependence characteristic of antiferromagnets with easy-plane anisotropy [11],

$$\left(\frac{\nu_\parallel}{\gamma_\parallel}\right)^2 = 2H_E|H_A'| + H_0^2. \tag{3}$$

Here, $H_A' < 0$ is the anisotropy field in the induced easy-plane state. The solid line in Fig. 1 for oscillation branch *2* corresponds to this equation with an energy gap $\nu_{c2} = \gamma_\parallel\sqrt{2H_E|H_A'|} = 16.5 \pm 0.5$ GHz. It follows that the magnetization jump observed in [8] in the magnetic field $H_c = 6.15$ kOe aligned with the principal axis is the magnetic field-induced spin-reorientation transition from the easy-axis to the easy-plane state rather than the spin flop transition in the easy-axis $GdFe_3(BO_3)_4$ phase. This magnetization jump is then caused by the transition from parallel susceptibility $\chi_\parallel$ to perpendicular susceptibility $\chi_\perp$, which is much larger in magnitude. According to the antiferromagnetic resonance and magnetic [8] measurements, the temperature dependence of the critical field shown in Fig. 3 by triangles is the phase boundary separating these two states on the plane temperature–magnetic field along the c axis.

The conclusion that the low-temperature state of the $GdFe_3(BO_3)_4$ crystal in the region of low fields is an easy-axis state is also substantiated by magnetic resonance in the field oriented in the basal plane. The frequency–field dependence at $H_A \ll H_E$ then takes the form [11]

$$\left(\frac{\nu_{\perp 1}}{\gamma_\perp}\right)^2 = (2H_E + H_A)H_A + \frac{2H_E - H_A}{2H_E + H_A}H_0^2 \approx (2H_E + H_A)H_A + H_0^2, \quad \left(\frac{\nu_{\perp 2}}{\gamma_\perp}\right)^2 = (2H_E + H_A)H_A - \frac{H_A}{2H_E + H_A}H_0^2. \tag{4}$$

The first equation describes oscillation branch *1* (Fig. 2), whose frequency increases as the field grows. Solid line *1* in Fig. 2 is the theoretical dependence of $\nu_{\perp 1}$ with the parameters $\nu_{\perp c} = \gamma_\perp\sqrt{(2H_E + H_A)H_A} = 29.0 \pm 0.2$ GHz and $\gamma_\perp = 2.66$ MHz/Oe; the $\nu_{\perp c}$ value coincides with $\nu_{\parallel c}$ for $H \parallel c$.

We found that a magnetic field applied in the basal plane of the crystal can also induce the transition to the easy-plane state. In this state, the frequency–field dependences of antiferromagnetic resonance for a magnetic field in the basal plane take the form [11]

$$\frac{\nu_{\perp 1}}{\gamma_\perp} = H_0\sqrt{1 + \frac{|H_A'|}{2H_E}} \approx H_0, \quad \left(\frac{\nu_{\perp 2}}{\gamma_\perp}\right)^2 = 2H_E|H_A'| - \frac{|H_A'|}{2H_E}H_0^2, \tag{5}$$

where magnetic anisotropy in this plane, which is weak according to the antiferromagnetic resonance data, is ignored.

The frequency–field dependences for the $\nu_{\perp 1}$ branches in the easy-plane and easy-axis states are

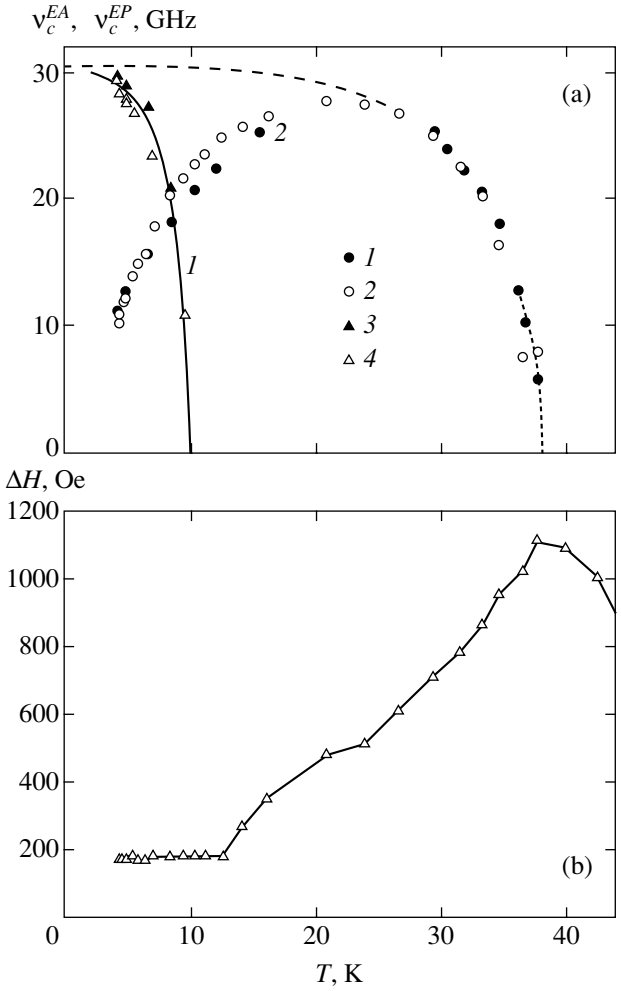

Fig. 6. (a) Temperature dependence of the energy gaps in the spectra of the (*1*) easy-axis and (*2*) easy-plane states. Frequencies and magnetic field orientations: (*1*) 26.11 GHz, **H** ∥ *c*; (*2*) 44.48 GHz, **H** ∥ *c*; (*3*) 26.11 GHz, **H** ∥ *c*; and (*4*) 38.63 GHz, **H** ⊥ *c*. (b) Temperature dependence of antiferromagnetic resonance line width at a 44.48 GHz and **H** ∥ c.

sharply different. Because of the presence of a gap in the spectrum of oscillations, the resonance field in the easy-axis state is always lower than in the state with an easy-plane anisotropy. The transformation of the resonance spectrum caused by heating the crystal (see Fig. 5) is just the transition between the $\nu_{\perp 1}$ oscillation branches of the easy-axis and easy-plane states.

It follows that the temperature dependence of the critical field shown in Fig. 4 is the phase boundary between the states with easy-axis and easy-plane anisotropies on the plane temperature–magnetic field in the basal plane. The temperature dependence of resonance fields for the $\nu_{\perp 1}$ branch in the easy-axis state of the crystal is caused by the temperature dependence of the energy gap in spectrum (4). In the easy-plane state, the resonance field for $\nu_{\perp 1}$ is temperature-independent according to (5). Resonance branch *2* in Fig. 2 corresponds to just this oscillation branch of the induced easy-plane phase.

Using (1) and (4), we can calculate the temperature dependences of the energy gaps ν_c^{EA} and ν_c^{EP} for the easy-axis and easy-plane states, respectively, from the temperature dependences of resonance fields (Fig. 3). The results are shown in Fig. 6a, which also contains the temperature dependence of ν_c^{EA} obtained from the temperature dependence of resonance absorption measured at 38.63 GHz for field $H \perp c$. These results closely agree with those obtained for $H \parallel c$. The energy gap ν_c^{EA} (curve *1*) tends to zero as the temperature approaches $T = 10$ K. It follows that the uniaxial anisotropy field H_A does indeed change sign at this temperature, and a spontaneous spin-reorientation transition occurs. The anomaly of magnetic properties close to 10 K observed in [8] is related to just this phase transition.

The temperature dependence of the energy gap ν_c^{EP} (Fig. 6a, curve *2*) has an unusual form. The gap first increases as the temperature grows, reaches a plateau at about 20 K, and then decreases to zero as the temperature approaches $T = 38$ K. Apparently, this is the temperature of magnetic ordering of the subsystem of iron ions, because spontaneous ordering of the subsystem of rare-earth metal ions usually occurs at much lower temperatures [1, 12]. The boundary between the paramagnetic state of the crystal and the ordered state of the iron subsystem is shown by dashed line *5* in the phase diagram (Fig. 3). The ground state of the iron subsystem is antiferromagnetic, and its anisotropy is of the easy-plane type. An increase in the energy gap as the temperature decreases from $T_N = 38$ K is typical of antiferromagnets. It is caused by an increase in the effective exchange and anisotropy fields as the crystal is cooled. In the absence of a rare-earth metal subsystem, the temperature dependence of the energy gap would reach a plateau below approximately 15–20 K, and the gap would remain virtually unchanged during cooling to 0 K, as is shown by the dashed line in the figure. It is reasonable to suggest that a decrease in the energy gap starting with about 20 K is related to the influence of the gadolinium subsystem. It is likely that this subsystem has the opposite anisotropy sign, its contribution to the total anisotropy increases in magnitude as the temperature lowers, and spontaneous reorientation from the easy-plane to the easy-axis state occurs at $T = 10$ K.

As concerns the supposed state of the gadolinium subsystem in this temperature region, it cannot be entirely ruled out that this subsystem experiences ordering precisely at about $T = 20$ K. Apart from the strong line broadening as the iron subsystem approaches the Néel temperature $T_N = 38$ K, we observe an obvious broadening in the region of 20 K, see the temperature dependence of line width (Fig. 6b) measured at a frequency of 44.48 GHz for $H \parallel c$. This broad-

ening can be caused by spontaneous ordering in the gadolinium subsystem. However, no magnetic property anomalies were detected at this temperature [8]. In addition, an analysis of the crystallographic structure (see below) leads us to suggest that indirect exchange interaction in the gadolinium subsystem is fairly weak. Lastly, it should be mentioned that, according to magnetic measurements, spontaneous ordering of the gadolinium subsystem in the $GdGa_3(BO_3)_4$ crystal, where all iron ions are replaced by diamagnetic ions, does not occur even at $T = 4.2$ K [13]. For this reason, the gadolinium subsystem should rather be treated as polarized by a biasing field created as a result of Fe^{3+}–Gd^{3+} exchange interaction over the whole temperature range of magnetic order studied, 4.2–38 K.

The suggestion of the polarization of the rare-earth metal subsystem and its influence on crystallographic anisotropy at low temperatures is substantiated by the results obtained in analyzing the gadolinium ferroborate crystal structure and exchange interactions. The crystal structure of rare-earth metal ferroborates is rhombohedral, space group $R32$ at room temperature [5, 6]. The lattice parameters are $a = 9.567(3)$ Å and $c = 7.578(2)$ Å [5], and the unit cell contains three $GdFe_3(BO_3)_4$ molecules. The Fe^{3+} ions have an oxygen environment in the form of slightly distorted octahedra. Neighboring octahedra share edges to produce a helicoidal chain along the c axis. The oxygen environment of Gd^{3+} is a distorted triangular prism sharing vertex oxygen atoms with Fe–O_6 octahedra of three neighboring helicoidal chains. A fragment of the crystal structure of $GdFe_3(BO_3)_4$ is shown in Fig. 7a, where two chains of Fe–O_6 octahedra and two adjacent Gd–O_6 prisms are shown. Two neighboring iron ions in a chain are coupled by indirect Fe–O–Fe exchange interaction through two oxygen ions with bond angles of 101.10° and 103.43°. The estimates obtained using the simple model of exchange coupling [14] show that exchange interactions between iron ions in chains are antiferromagnetic and the exchange integral value is $J^{Fe\text{–}Fe} \approx -9$ K. Neighboring chains interact with each other through the Fe–O–Gd–O–Fe bonds and B–O_3 complexes shown as triangles in the figure. Judging from the absence of a broad maximum of the temperature dependence of magnetic susceptibility characteristic of low-dimensional magnetism [8], these interchain interactions are sufficiently strong for the establishment of three-dimensional magnetic order in the iron subsystem.

If the structure of gadolinium ferroborate is treated as planes containing iron and gadolinium ions that alternate along the c axis, then each gadolinium ion is coupled by indirect Gd–O–Fe interactions with iron ions of two neighboring planes that belong to one sublattice and is not coupled with iron ions of its own plane that form another sublattice. According to estimates obtained by following [14], Gd–O–Fe exchange interactions that polarize the gadolinium subsystem at $T < T_N$ are also antiferromagnetic and are weaker than exchange interactions in the iron subsystem. These interactions are weak because the distance between the gadolinium and oxygen ions $R_{Gd\text{–}O} = 2.4$ Å in this chain is much larger than the Fe–O distances, $R_{Fe\text{–}O} = 1.99$–2.04 Å. It is likely, however, that polarizing exchange coupling between the iron and rare-earth metal ions in the hantite structure, that is, in $GdFe_3(BO_3)_4$, is stronger than similar coupling in rare-earth metal orthoferrites, where rare-earth metal ions interact with iron ions from different sublattices, which results in almost complete isotropic exchange balancing [1, 15, 16].

The gadolinium ions are in turn coupled with each other only through B–O_3 complexes. Both arms in the Gd–BO_3–Gd interaction chain are fairly long, $R_{Gd\text{–}O} = 2.4$ Å. It appears that indirect exchange coupling in the gadolinium subsystem is for this reason weaker than the polarizing action of the iron subsystem, which explains the absence of spontaneous magnetic ordering in the gadolinium subsystem of $GdGa_3(BO_3)_4$ even at $T = 4.2$ K.

A consideration of all these special features leads us to suggest that the $GdFe_3(BO_3)_4$ crystal at low temperatures has the magnetic structure shown in Fig. 7b. This structure consists of planes perpendicular to the c axis and alternating along it. The planes contain ferromagnetically ordered iron and gadolinium ions. Neighboring planes are ordered antiferromagnetically. The size of the magnetic unit cell is doubled along the c axis compared with the crystal lattice cell.

It follows that the magnetic anisotropic properties of gadolinium ferroborate at low temperatures are formed in the competition between anisotropic interactions of iron and gadolinium ion subsystems, which have different anisotropy signs. The iron subsystem is a collinear two-sublattice antiferromagnetic subsystem spontaneously ordered at $T < T_N = 38$ K. The gadolinium subsystem is polarized by antiferromagnetic interactions with the iron subsystem and can also be divided into two sublattices.

This view on the magnetic structure of gadolinium ferroborate allows us to write the energy of this crystal in the presence of a magnetic field as

$$U = J_{11}\mathbf{M}_1 \cdot \mathbf{M}_2 + J_{12}(\mathbf{M}_1 \cdot \mathbf{m}_1 + \mathbf{M}_2 \cdot \mathbf{m}_2) - \frac{K_1}{2M_0^2}(M_{1z}^2 + M_{2z}^2) - \frac{K_2}{2m_0^2}(m_{1z}^2 + m_{2z}^2) - \mathbf{H} \cdot (\mathbf{M}_1 + \mathbf{M}_2 + \mathbf{m}_1 + \mathbf{m}_2). \quad (6)$$

Here, $J_1 > 0$ and $J_{12} > 0$ are the exchange coupling parameters in the iron subsystem and between the iron and gadolinium subsystems, respectively; $\mathbf{M}_{1,2}$ and $\mathbf{m}_{1,2}$ are the magnetic moments of the iron and gadolinium subsystem sublattices, $|\mathbf{M}_1| = |\mathbf{M}_2| = M_0$ and $|\mathbf{m}_1| = |\mathbf{m}_2| = m_0$; and K_1 and K_2 are the uniaxial anisotropy

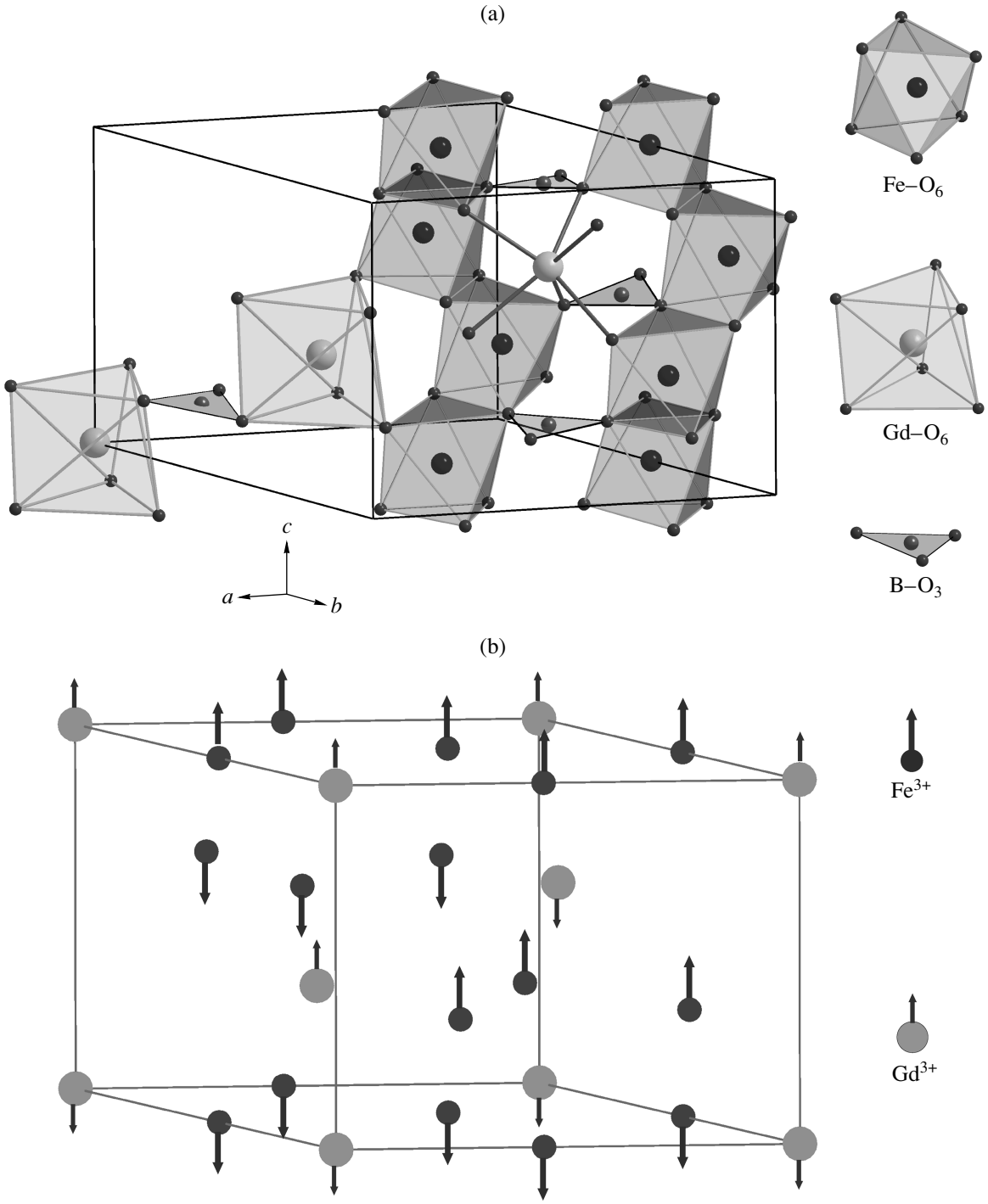

Fig. 7. (a) Fragment of the crystal structure of $GdFe_3(BO_3)_4$ and (b) supposed magnetic structure of $GdFe_3(BO_3)_4$ at $T < 10$ K.

constants of the iron and gadolinium subsystems. It follows from the experimental data that $K_1 < 0$ and $K_2 > 0$. Exchange coupling in the gadolinium subsystem and anisotropy in the basal plane are ignored. In addition, the second energy term is written on the assumption that the ions of each iron sublattice only interact with ions of one gadolinium sublattice. The minimization of energy (6) in the absence of a magnetic field gives the following solutions for polar angles θ_i and η_i and sublattice magnetic moments $\mathbf{M}_i$ and $\mathbf{m}_i$:

1) $\theta_1 = 0$, $\theta_2 = \pi$, $\eta_1 = \pi$, $\eta_2 = 0$;

2) $\theta_1 = \pi/2$, $\theta_2 = -\pi/2$, $\eta_1 = -\pi/2$, $\eta_2 = \pi/2$;

3) $\theta_1 = \theta$, $\theta_2 = \pi + \theta$, $\eta_1 = \pi + \eta$, $\eta_2 = \eta$.

Generally, θ and η are not equal to each other and to 0 and π/2.

The last solution describes the angular phase in the narrow region $K_2 \approx |K_1|$, more exactly, in the region bounded by the inequalities

$$K_1' < K_2 < K_1'',$$

$$K_1' = |K_1|\frac{\cos^2\theta}{\cos^2\eta} + 2J_{12}mM\frac{1-\cos(\theta-\eta)}{\cos^2\eta}, \quad (7)$$

$$K_1'' = |K_1|\frac{\sin^2\theta}{\sin^2\eta} - 2J_{12}mM\frac{1-\cos(\theta-\eta)}{\sin^2\eta}.$$

Outside this region, we have the state with an easy-axis anisotropy if $K_2 > |K_1|$ [solution (1)] or the state with an easy-plane anisotropy [solution (2)].

It follows that the sequence of changes in the magnetic state of gadolinium ferroborate as the temperature lowers in the absence of a magnetic field can be explained as follows. The crystal is a two-sublattice antiferromagnet with an easy-plane anisotropy in the region of 20–38 K, where only the subsystem of iron ions is predominantly ordered. The degree of the polarization of the gadolinium subsystem with the opposite anisotropy sign increases as the temperature lowers; accordingly, the contribution of this subsystem to the total crystal anisotropy grows. This contribution becomes noticeable at temperatures lower than 20 K, and, at $T = 10$ K, the total anisotropy energy changes sign. The anisotropy fields H_A and H_A' present in equations (1)–(5) for antiferromagnetic resonance frequencies are resultant anisotropy fields at temperatures below 20 K; they are determined by the contributions of both magnetic subsystems. The magnetic structure of $GdFe_3(BO_3)_4$ shown in Fig. 7b corresponds to low temperatures.

This model can be used to estimate the anisotropy fields of both magnetic subsystems of gadolinium ferroborate at $T = 4.2$ K. Using the experimental exchange field value $H_E = 180$ kOe obtained from perpendicular susceptibility at $T = 4.2$ K [8] and the energy gap in the spectrum extrapolated to low temperatures $\nu_c \approx 30$ GHz for the iron subsystem (see Fig. 6a), we obtain the anisotropy field for the iron subsystem at low temperatures $H_A^{Fe} \approx -320$ Oe. The experimental energy gap 29.4 GHz value for the easy-axis crystal state at $T =$ 4.2 K, which is determined by the resultant anisotropy field $H_A \approx 310$ Oe, can be used to estimate the anisotropy field for the gadolinium subsystem at the helium temperature, $H_A^{Gd} \approx 630$ Oe.

A magnetic field changes the orientations of the magnetic moments of the sublattices of both subsystems, primarily the gadolinium subsystem coupled by comparatively weak exchange interaction with the iron subsystem. Moreover, further calculations show that, in very strong magnetic fields, the gadolinium subsystem experiences the transition from the polarized antiferromagnetic to the "collapsed" spin-flip state. This changes the ratio between the contributions of the iron and gadolinium subsystems to the total anisotropy. As a result, the temperature of the orientation transition should also change as the magnetic field increases, and the very transition between the easy-axis and easy-plane states can occur under changes not only in temperature but also in magnetic field. The dependences of the equilibrium polar angles θ_1 and η_2 on the magnetic field along axis c obtained by numerically minimizing crystal energy (6) are shown in Fig. 8. The minimization was performed using the following potential parameter values:

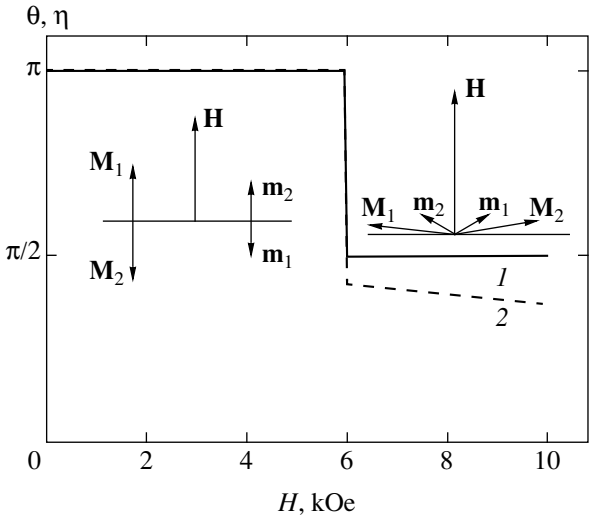

Fig. 8. Field dependence of equilibrium polar angles of the (*1*) iron and (*2*) gadolinium sublattice magnetic moments.

$$J_1 = 2400, \quad J_{12} = 320, \quad K_1 = -24000 \text{ erg/cm}^3,$$

$$K_2 = 62000 \text{ erg/cm}^3, \quad M_0 = 75 \text{ G cm}^3/\text{g},$$

$$m_0 = 25 \text{ G cm}^3/\text{g}.$$

The exchange parameter $J_1 = H_E/M_0$ and the anisotropy constant $K_1 = H_A^{Fe}M_0$ were calculated from the exchange field $H_E = 180$ kOe and the anisotropy field of the iron subsystem $H_A^{Fe} \approx -320$ Oe given above, and the J_{12}, K_2, and m_0 values played the role of adjustment parameters. The magnetization of the gadolinium subsystem sublattice was taken to be smaller than the saturation value $m_0 = 35$ G cm^3/g. Because of weak exchange interactions with the iron subsystem, the gadolinium subsystem was considered unsaturated at $T =$ 4.2 K (this is the temperature at which the calculation results were compared with the experimental data). For

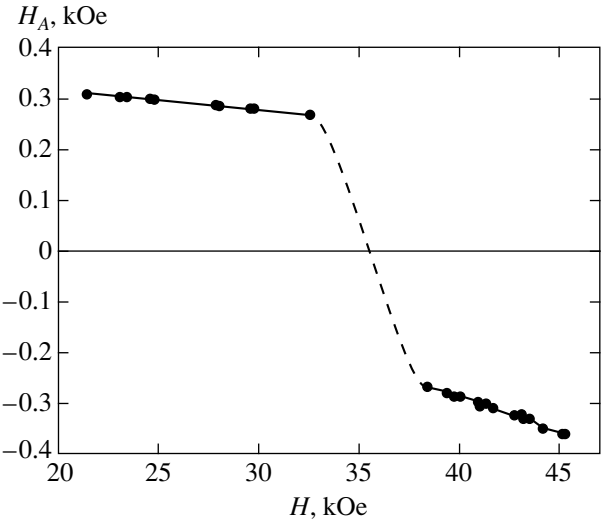

Fig. 9. Field dependence of the resultant anisotropy field for $H \perp c$ at $T = 4.2$ K.

the same reason, the magnetic moments of the sublattices in the gadolinium subsystem "collapse" in a magnetic field more rapidly than the iron sublattice moments, see Fig. 8.

Calculations show that, at this set of parameters, the transition from the easy-axis to the easy-plane state occurs in a magnetic field of $H_c = 5.92$ kOe. This value is close to the experimental critical field values obtained from antiferromagnetic resonance and magnetic measurements [8]. Also note that, according to our calculations, magnetic moment reorientation occurs in a jump, without the formation of an angular phase.

If the magnetic field is directed in the basal plane of the crystal, field-induced spin reorientation occurs via an angular phase at the same thermodynamic potential parameters. This phase exists in the interval of magnetic fields from 30.2 to 33.8 kOe (the larger value is labeled by an asterisk in Fig. 4). Within this interval, which is in agreement with the antiferromagnetic resonance data, the antiferromagnetic vectors of both magnetic subsystems rotate in the plane perpendicular to the magnetic field. According to the magnetic measurements [8, 13], this transition extends from 30.8 to 33.5 kOe at $T = 4.2$ K and has no field hysteresis, which also closely agrees with the results of our calculations.

The suggestion of the field dependence of the resultant anisotropy field of gadolinium ferroborate allows the unusual character of frequency–field dependences *2* and *3* (Fig. 2) to be explained. As they are situated above and below the critical spin reorientation field, it is reasonable to suggest that these dependences correspond to oscillations $\nu_{\perp 2}$ of the easy-axis and field-induced easy-plane states. A comparison of Eqs. (4) and (5) shows that the oscillation frequencies $\nu_{\perp 2}$ in both states virtually identically depend on the magnetic field because $|H_A| \ll H_E$. Using the exchange field $H_E \approx 180$ kOe and the experimental energy gap value, 29 GHz, we find that the $H_A/2H_E$ ratio, which determines the steepness of the frequency–field dependence for this branch, is about 2×10^{-4}. This value was used in Fig. 2 to plot the frequency–field dependence of $\nu_{\perp 2}$ [Eq. (4)] for the easy-axis state (the dashed line). On the scale of the figure, this branch can be considered magnetic-field–independent. As concerns the experimentally observed fairly strong magnetic field dependence of resonance frequencies, it probably originates from changes in the energy gaps in the spectrum caused by the field dependence of the resultant anisotropy and determined by the competing contributions of the iron and gadolinium subsystems. The field dependence of the resultant uniaxial anisotropy field calculated on the basis of these considerations is shown in Fig. 9.

Also note that the suggestion of competitive contributions of the iron and gadolinium subsystems to the uniaxial anisotropy of $GdFe_3(BO_3)_4$ is qualitatively substantiated by the magnetic resonance data on $GdFe_{3-x}Ga_x(BO_3)_4$ ($x \approx 1$) crystals. Partial substitution of iron ions by diamagnetic gallium ions decreases the contribution of the iron subsystem to anisotropy. For this reason, the total anisotropy and energy gap at 4.2 K increase compared with pure $GdFe_3(BO_3)_4$ (see inset to Fig. 1), and the critical field of the transition to the easy-plane state for $\mathbf{H} \parallel c$ increases from 6.0 to 9.3 kOe at $T = 4.2$ K.

4. CONCLUSIONS

To summarize, we thoroughly studied antiferromagnetic resonance and magnetic phase transitions in gadolinium ferroborate $GdFe_3(BO_3)_4$. This is the first such study for rare-earth metal magnets with hantite structures. An analysis of the experimental data led us to the following conclusions on the magnetic structure of this compound.

Ordering of the subsystem of iron ions, which is a two-sublattice antiferromagnet with easy-plane anisotropy, occurs at the Néel temperature $T_N = 38$ K. In our view, the influence of the anisotropy of the gadolinium subsystem polarized by exchange interaction with the iron subsystem becomes noticeable as the temperature decreases to 20 K. The gadolinium subsystem can also be represented in the form of a two-sublattice antiferromagnet with easy-axis anisotropy at temperatures below 20 K. The competition of the anisotropic contributions of the iron and gadolinium subsystems results in a spontaneous transition from the easy-plane to the easy-axis state as the temperature decreases to $T = 10$ K. An analysis of the crystal structure and exchange interactions at temperatures below 20 K led us to suggest the magnetic structure of $GdFe_3(BO_3)_4$ comprising planes that contain ferromagnetically ordered iron and gadolinium ions, are perpendicular to the c axis, and alternate along this axis. The neighboring planes are

ordered antiferromagnetically. The size of the magnetic unit cell along the *c* axis equals two times the size of the crystallographic unit cell.

It follows from the resonance data that transitions between the easy-axis and easy-plane states occur not only depending on the temperature but also as the magnetic field changes. We constructed the experimental magnetic phase diagrams for magnetic fields oriented along the crystal axis and in the basal plane.

A simple model was suggested to describe spontaneous and induced phase transitions. The model takes into account antiferromagnetic exchange interactions within the iron subsystem and between the iron and gadolinium subsystems, the anisotropy energies of both subsystems, and the Zeeman energy. This model was used to find the conditions of the existence of the easy-axis, easy-plane, and angular phases. Calculations were performed to determine the critical fields of spin reorientation transitions in magnetic fields along the crystal axis and in the basal plane. The results were in close agreement with the experimental data obtained at $T = 4.2$ K.

ACKNOWLEDGMENTS

The authors thank M.A. Popov for useful discussions.

REFERENCES

1. K. P. Belov, A. K. Zvezdin, A. M. Kadomtseva, and R. Z. Levitin, *Reorientational Transitions in Rare-Earth Magnets* (Nauka, Moscow, 1979) [in Russian].
2. A. D. Mills, Inorg. Chem. **1**, 960 (1962).
3. G. Blasse and A. Bril, Phys. Status Solidi **20**, 551 (1967).
4. V. I. Chani, M. I. Timoshechkin, K. Inoue, *et al.*, Inorg. Mater. **30**, 1466 (1992).
5. N. I. Leonyuk and L. I. Leonyuk, Prog. Cryst. Growth Charact. Mater. **31**, 179 (1995).
6. J. A. Campa, C. Cascales, E. Guttierez-Puebla, *et al.*, Chem. Mater. **9**, 237 (1997).
7. Y. Hinatsu, Y. Doi, K. Ito, *et al.*, J. Solid State Chem. **172**, 438 (2003).
8. A. D. Balaev, L. N. Bezmaternykh, I. A. Gudim, *et al.*, J. Magn. Magn. Mater. **258–259**, 532 (2003).
9. V. I. Tugarinov, I. Ya. Makievskiĭ, and A. I. Pankrats, Prib. Tekh. Éksp., No. 4 (2004) [Instrum. Exp. Tech. **47**, 472 (2004)].
10. I. S. Jackobs, R. A. Beyerline, S. Foner, and J. P. Remeika, Int. J. Magn. **1**, 193 (1971).
11. A. G. Gurevich, *Magnetic Resonance in Ferrites and Antiferromagnets* (Nauka, Moscow, 1973) [in Russian].
12. A. K. Zvezdin, V. M. Matveev, A. A. Mukhin, and A. I. Popov, *Rare-Earth Ions in Magnetic-Ordered Crystals* (Nauka, Moscow, 1985) [in Russian].
13. A. D. Balaev, private communication.
14. O. A. Bayukov and A. F. Savitskiĭ, Fiz. Tverd. Tela (St. Petersburg) **36**, 1923 (1994) [Phys. Solid State **36**, 1049 (1994)].
15. D. V. Belov, A. K. Zvezdin, A. M. Kadomtseva, *et al.*, Fiz. Tverd. Tela (Leningrad) **23**, 2831 (1981) [Sov. Phys. Solid State **23**, 1654 (1981)].
16. J. D. Cashion, A. H. Cooke, D. M. Martin, and M. R. Wells, J. Phys. C: Solid State Phys. **3**, 1612 (1970).

Translated by V. Sipachev